ACADÉMIE
DES SCIENCES
INSTITUT DE FRANCE

Comptes Rendus
Mécanique

Emilio Turco

Heavy changes in pantograph mechanics with slight repositioning of nodes

Volume 354 (2026), p. 183-201

Online since: 18 March 2026

https://doi.org/10.5802/crmeca.352

The Comptes Rendus. Mécanique *are a member of the Mersenne Center for open scientific publishing*
www.centre-mersenne.org — e-ISSN : 1873-7234

ACADÉMIE DES SCIENCES
INSTITUT DE FRANCE

Comptes Rendus. Mécanique
2026, Vol. 354, p. 183-201
https://doi.org/10.5802/crmeca.352

Research article

Heavy changes in pantograph mechanics with slight repositioning of nodes

Emilio Turco [a]

[a] Department of Architecture, Design and Urban planning – DADU, University of Sassari, Asilo Sella, via Garibaldi 35, 07041, Alghero (SS), Italy

E-mail: emilio.turco@uniss.it

Abstract. Pantographic unit cells are well-known and used both for deployable structures and metamaterials design. It is surely less known that with minor changes, moving the nodes in the reference configuration or using angulated elements, this unit cells can be used to build curved shapes in the strain-free configuration. Curved pantographs are employable in several technical applications. One interesting application is related with robot arms. The peculiar characteristic of pantographic structures, linear or curved, is the existence of a floppy mode, i.e. a zero energy mode, which ensures the existence of a branch of the equilibrium path without strain in all its parts. This characteristic provides the deployability of the pantographic structures and several exotic mechanical behaviours in metamaterials based on the same pattern. We discuss some results obtained by a mechanical digital twin capable of: (i) verifying the deployability, i.e. the existence of a floppy mode when it is not prevented by constraints, of the considered scheme checking for the whole equilibrium path the absence of strain on all the springs modelling the problem; (ii) providing some information, useful for a preliminary structural design, about the mechanical behaviour of a simple structural scheme in the hypothesis of large displacements when the floppy mode is prevented by a large enough number of constraints.

Keywords. Mechanics of curved pantographs, large displacement analysis, discrete element model, deployable structures.

Note. Article submitted by invitation.

Manuscript received 20 November 2025, revised and accepted 24 February 2026, online since 18 March 2026.

1. Introduction

Pantographic structures have been extensively studied in the last years for their exotic properties when used to design metamaterials, see, e.g., [1,2] for a broad overview on the theme. Initially conceived as an example of second gradient structures, i.e. structures in which the strain energy also depends on the second gradient of the displacement field [3], therefore to give an example capable of justifying the existence of structures of this kind. The peculiar characteristic of the pantographic structures is the existence of a floppy mode — i.e. a zero energy mode — in the unit cell which makes them suitable, besides being very interesting in the design of metamaterials [4–6], for the design of deployable structures. We remark that there exist other articulated mechanisms capable of generating complex kinematics, see e.g. [7]. The latter differs from those discussed here mainly for the reference configuration, rectilinear vs. circular, and for the fundamental *bricks* used, i.e. springs vs. springs and angle springs.

In the work of You and Pellegrino concerning deployable structures, [8], there is an excellent introduction to this kind of structures — also known as scissor-like structures — with an extensive bibliography mostly concerning deployable structures. The concept of pantographic unit cell is generalised discussing different kinds of unit cells, see those reported schematically in Figure 1. In the field of deployable structures this concept, also extended in three-dimensions, is found, e.g., in the deployable theatre roof of Piñero [9] and in the Hoberman sphere, see [10,11].

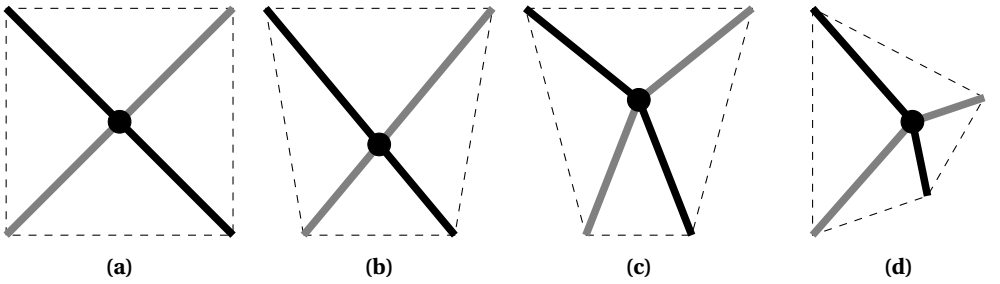

Figure 1. Four different kinds of pantographic unit cells: (a) ordinary, (b) Piñero, (c) Hoberman and (d) Hoberman modified.

From left to right, the first one is the most known pantographic unit cell: it has two axes of symmetry and the pivot, depicted with a black bullet, connects two straight beams splitting them in four equal segments also known as arms (segments in-between the unit cell vertices and the pivot). The second has only one axis of symmetry and the pivot splits each one of the two straight beams in two unequal arms. The third one has again one axis of symmetry but the pivot splits the two angulated beams in four segments of equal length. The last one has no axis of symmetry and the pivot splits the two angulated beams in four unequal arms.

The unit cells depicted in Figure 1 can be assembled side-by-side by means of hinges to obtain straight structures in the case of ordinary pantographic unit cell or curved structures in the case of Piñero or Hoberman unit cells. The last unit cell, known as Hoberman modified, in order to be assembled in a structure requires a preliminary reflection about the connection side. Also in this last case the assembled structure is curved. We remark that the first two unit cells are formed by straight beams whereas the last two by angulated beams.

You and Pellegrino, always in the already cited paper [8], state: (i) the assembly of unit cells having each one a floppy mode does not ensure the deployability of the whole structure; (ii) it is also required that the interfaces between unit cells deform in a compatible fashion. As a consequence, any assembly of unit cells admitting a floppy mode has to be checked in the whole fold-unfold process. We further remark that this process involves large displacements and, as a consequence, it requires a nonlinear analysis to solve the equilibrium problem. The whole process, especially for three-dimensional structures, can be rather expensive from the computational point of view.[1]

It follows that the only way to check if a structure made by a suitable number of unit cells can be assumed as deployable is to test if in all the configurations between the folded and the unfolded structure, and vice versa, are strain-free. In other words, it is necessary to perform a Gedanken experiment, see, e.g., [13], from the computational point of view. A simple example on a well-known structure can clarify this concept. We consider a pantographic structure made by ten square pantographic unit cells, see Figure 1(a). It is well-known and also simple to prove that the whole process is strain-free. The six plots in Figure 2 report some configurations — from

[1] Although a continuum approach is not considered in this work, the author believes that analogous results can be obtained using third gradient continuum models as it is shown in [12].

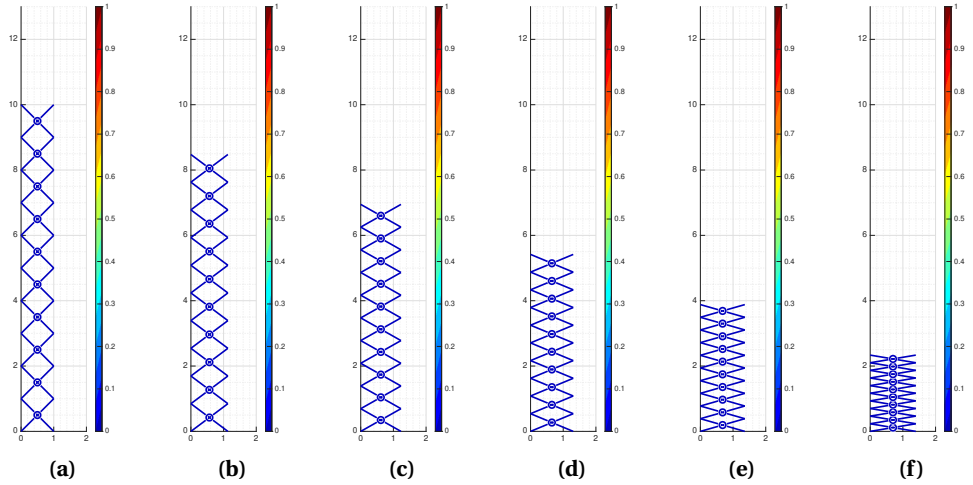

Figure 2. Floppy mode of a pantographic structure based on the ordinary unit cell (a)–(f).

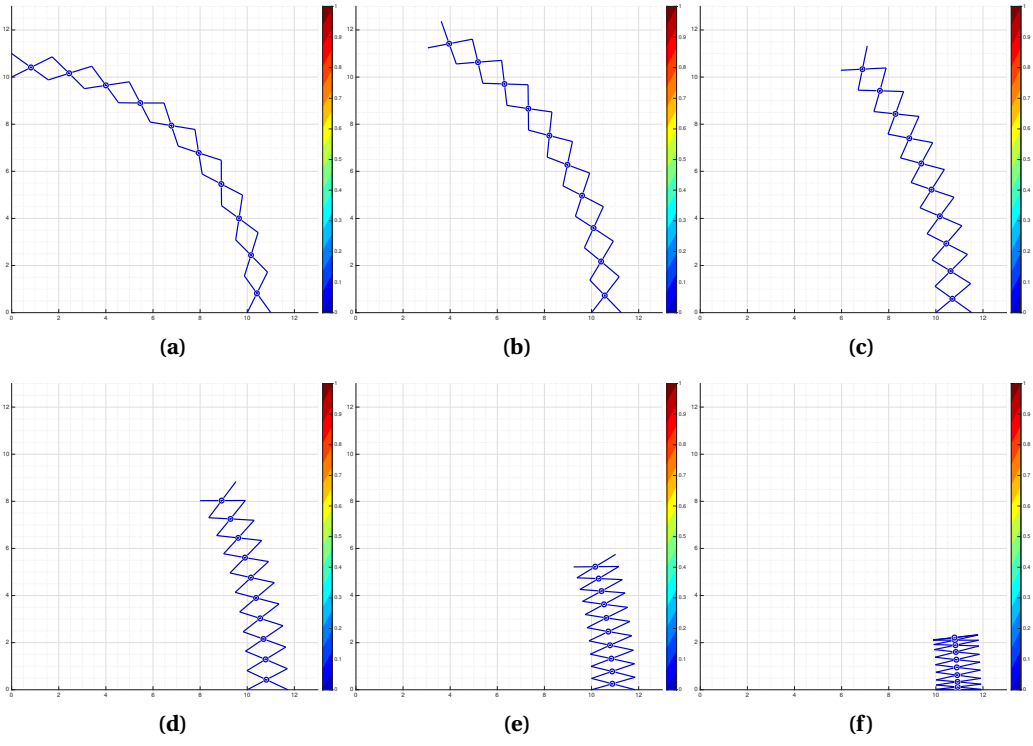

Figure 3. Floppy mode of a pantographic structure based on the Piñero unit cell (a)–(f).

unfold to fold configurations — deriving from a nonlinear analysis realised with the tool sketched in Section 2. The performed numerical simulation is obtained simply by constraining the bottom left node of the pantograph and moving to the right the bottom right node. The color bar defining the strain energy level in each part of the pantographic structure shows, as expected, that in all the six configurations of the floppy mode the strain energy level is zero (blue color).

Somewhat different is the floppy mode corresponding to a pantograph obtained by an assembly of ten Piñero unit cells, see Figure 1(b). Figure 3 shows the floppy mode of the system. It is obtained performing again a numerical simulation with the same conditions of the straight pantograph: constraining the bottom left node of the pantograph and moving to the right the bottom right node. The considered geometry, circular with prescribed inner and outer radii, permits to compute in a straightforward way the pivot position of the unit cell by using the analytical relation reported in Section 4. The stroboscopic shoots reported in Figure 3 show that the whole process does not produce strain energy, as shown by the color bar, in any element of the pantographic arc structure.

Keeping in mind the argument sketched in the foregoing, in the forthcoming sections we describe: (i) a very simple model capable of performing the nonlinear analysis of a discrete system made of N points linked by springs connecting two of them and by angle spring connecting three of them [14–16], Section 2; (ii) a simple but refined strategy capable of solving the nonlinear system of equilibrium equations both when the floppy mode is free to revealing and when it is prevented by an enough number of constraints, Section 3; (iii) some numerical simulations concerning Piñero and Hoberman unit cells, Section 4; and (iv) some concluding remarks and future challenges, Section 5.

2. Strain energy of a spring network

In the framework of the total potential energy minimum, see [17,18], the mechanical behaviour of a system of N points can be described by defining the strain energy associated with the s-th spring connecting the points i and j and the angle strain energy associated with the t-th angle spring connecting i, j and h points.

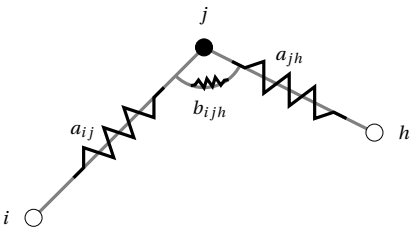

Figure 4. Spring and angle spring mechanical interactions for the basic elements.

The strain energy associated with the s-th spring is defined as

$$A_s = \frac{1}{2} a_s (\ell_s - L_s)^2, \tag{1}$$

where a_s, ℓ_s and L_s are the spring stiffness, the current and the reference lengths, respectively, and the so-called engineering strain measure is used.

Supposing that the points i and j have coordinates collected in the vectors $\mathbf{X}_i$ and $\mathbf{X}_j$ in the reference and $\mathbf{x}_i$ and $\mathbf{x}_j$ in the current configurations, respectively, then we define

$$\begin{aligned} \Delta\mathbf{X} &= \mathbf{X}_j - \mathbf{X}_i, \\ L_s &= \|\Delta\mathbf{X}\|, \\ \Delta\mathbf{x} &= \mathbf{x}_j - \mathbf{x}_i, \\ \ell_s &= \|\Delta\mathbf{x}\|. \end{aligned} \tag{2}$$

The reaction vector $\mathbf{r}_s$, defined as the gradient of the strain energy, can be computed as

$$\mathbf{r}_s = \frac{\mathrm{d}A_s}{\mathrm{d}\ell_s}\frac{\mathrm{d}\ell_s}{\mathrm{d}\mathbf{x}_s} = a_s(\ell_s - L_s)\frac{\mathrm{d}\ell_s}{\mathrm{d}\mathbf{x}_s}, \tag{3}$$

where

$$\mathbf{x}_s = \begin{bmatrix}\mathbf{x}_i \\ \mathbf{x}_j\end{bmatrix}. \tag{4}$$

The gradient of the current length ℓ_s can be determined without computing the derivatives but simply imposing the equilibrium equations. Since the axial force $N_s = a_s(\ell_s - L_s)$, the reaction vector is

$$\mathbf{r}_s = N\begin{bmatrix}-\mathbf{t}_s \\ \mathbf{t}_s\end{bmatrix}, \tag{5}$$

$\mathbf{t}_s = \Delta\mathbf{x}/\ell_s$ being the tangent unit vector in the current configuration.

The tangent stiffness matrix of the s-th element can be obtained by computing the gradient of the reaction, in formula

$$\mathbf{K}_s = \frac{\mathrm{d}\mathbf{r}_s}{\mathrm{d}\mathbf{x}_s} = \frac{\mathrm{d}\mathbf{r}_s}{\mathrm{d}\ell_s}\frac{\mathrm{d}\ell_s}{\mathrm{d}\mathbf{x}_s} = a_s\left(\left(\frac{\mathrm{d}\ell_s}{\mathrm{d}\mathbf{x}_s}\right)\left(\frac{\mathrm{d}\ell_s}{\mathrm{d}\mathbf{x}_s}\right)^T + (\ell_s - L_s)\frac{\mathrm{d}^2\ell_s}{\mathrm{d}\mathbf{x}_s^2}\right), \tag{6}$$

where the Hessian of the current length ℓ_s, i.e. $\frac{\mathrm{d}^2\ell_s}{\mathrm{d}\mathbf{x}_s^2}$, can be computed by using an algebraic manipulator in order to avoid cumbersome calculations.

The angle strain energy associated with the t-th angle spring is defined as

$$B_t = \frac{1}{2}b_t(\vartheta_t - \Theta_t)^2, \tag{7}$$

where b_t, ϑ_t and Θ_t are the angle stiffness, the current and the reference angles, respectively.

If we consider three nodes i, j and h and their coordinates $\mathbf{X}_i$, $\mathbf{X}_j$ and $\mathbf{X}_h$ in the reference and $\mathbf{x}_i$, $\mathbf{x}_j$ and $\mathbf{x}_h$ in the current configurations, the reaction vector associated to angle strain energy is

$$\mathbf{r}_t = \frac{\mathrm{d}B_t}{\mathrm{d}\mathbf{x}_t} = \frac{\mathrm{d}B_t}{\mathrm{d}\vartheta_t}\frac{\mathrm{d}\vartheta_t}{\mathrm{d}\mathbf{x}_t} = b_t(\vartheta_t - \Theta_t)\frac{\mathrm{d}\vartheta_t}{\mathrm{d}\mathbf{x}_t}, \tag{8}$$

where

$$\mathbf{x}_t = \begin{bmatrix}\mathbf{x}_i \\ \mathbf{x}_j \\ \mathbf{x}_h\end{bmatrix}. \tag{9}$$

The gradient of the current dihedral angle ϑ_t can be determined, again, by using the equilibrium since the moment produced by the angle spring is $M_t = b_t(\vartheta_t - \Theta_t)$. It derives

$$\nabla\vartheta_t = \begin{bmatrix}\frac{\mathbf{n}_{ji}}{\ell_{ji}} \\ -\frac{\mathbf{n}_{ji}}{\ell_{ji}} + \frac{\mathbf{n}_{jh}}{\ell_{jh}} \\ -\frac{\mathbf{n}_{jh}}{\ell_{jh}}\end{bmatrix}, \tag{10}$$

$\mathbf{n}_{ji}$ and $\mathbf{n}_{jh}$ being the unit vectors orthogonal to the unit tangent vectors $\mathbf{t}_{ji}$ and $\mathbf{t}_{jh}$. For instance, $\mathbf{n}_{ji} = \big(t_{ij}(2), -t_{ij}(1)\big)$.

The tangent stiffness matrix of the t-th element can be obtained by computing the gradient of the reaction.

$$\mathbf{K}_t = \frac{\mathrm{d}\mathbf{r}_t}{\mathrm{d}\mathbf{x}_t} = \frac{\mathrm{d}\mathbf{r}_s}{\mathrm{d}\vartheta_t}\frac{\mathrm{d}\vartheta_t}{\mathrm{d}\mathbf{x}_t} = b_t\left(\left(\frac{\mathrm{d}\vartheta_t}{\mathrm{d}\mathbf{x}_t}\right)\left(\frac{\mathrm{d}\vartheta_t}{\mathrm{d}\mathbf{x}_t}\right)^T + (\vartheta_t - \Theta_t)\frac{\mathrm{d}^2\vartheta_t}{\mathrm{d}\mathbf{x}_t^2}\right). \tag{11}$$

Also in this case, the Hessian of the current dihedral angle ϑ_t, i.e. $\frac{\mathrm{d}^2\vartheta_t}{\mathrm{d}\mathbf{x}_t^2}$, can be computed by using an algebraic manipulator in order to avoid cumbersome calculation. The interested reader could find an in-depth of this argument in two works about the origami mechanics [19,20] and the references therein.

If we collect in the vectors $\mathbf{X}$ and $\mathbf{x}$ the coordinates of the N points in the reference and in the current configurations, the minimum of the total potential energy, using its additivity property, gives the system of equilibrium equations

$$\mathbf{s}(\mathbf{x}) - \lambda\mathbf{p} = \mathbf{0}, \tag{12}$$

where $\mathbf{s}(\mathbf{x})$ is the structural reaction, or in brief the reaction, and $\lambda\mathbf{p}$ is the vector of the external forces ruled by the scalar parameter λ.

We remark that the strain energy definitions of spring and angle spring are the only tools necessary to define the strain energy of the spring network. No further remarks are necessary on the spring strain energy and its derivatives whereas the angle spring strain energy and its derivatives, as defined in the foregoing, can also be used if i, j and h are in-line. The way previously followed to compute the reaction vector and the stiffness matrix has the advantage to simplify the calculations using the physics of the problem but, overall, permits to avoid singularities in the expressions involved in the computations of the stiffness matrix.

3. Solving the large displacement problem

Due to the hypothesis of large displacements, when the nonlinear system of equilibrium equations (12) has to be solved an *ad hoc* procedure is necessary. By referring to [21] for a detailed explanation, here we recall that the discussed method simply uses three basic ingredients: (i) the Newton–Raphson method;[2] (ii) the Riks' arc-length strategy to bypass limit points eventually presents in the equilibrium path, see [23]; and (iii) the step-length adapter proposed by Clarke and Hancock [24].

We define the equilibrium path as a set of points $(\mathbf{x}_j, \lambda_j)$, $j = 0, 1, \ldots, N_{\text{steps}}$, solution of Eq. (12), i.e. when a suitable norm of the residue is less than a prefixed tolerance. We suppose that for the j-th point of the equilibrium path the solution pair $(\mathbf{x}, \lambda)$ is known and we are interested in the evaluation of the next equilibrium point $(\mathbf{x} + \Delta\mathbf{x}, \lambda + \Delta\lambda)$. We define the residue as

$$\mathbf{r} = \mathbf{s}(\mathbf{x}) - \lambda\mathbf{p}, \tag{13}$$

and expand it in Taylor series up to first order

$$\mathbf{r}(\mathbf{x} + \Delta\mathbf{x}) \approx \mathbf{r}(\mathbf{x}) + \mathbf{K}(\mathbf{x})\Delta\mathbf{x}, \tag{14}$$

where the stiffness matrix $\mathbf{K}(\mathbf{x})$ is the gradient of the reaction $\mathbf{s}(\mathbf{x})$. In order to slim the notation, we define $\mathbf{K}_\mathbf{x} := \mathbf{K}(\mathbf{x})$, $\mathbf{s}_\mathbf{x} := \mathbf{s}(\mathbf{x})$ and $\mathbf{r}_\mathbf{x} := \mathbf{r}(\mathbf{x})$. Imposing that the residue be zero gives the estimate of the correction $\Delta\mathbf{x}$

$$\Delta\mathbf{x} = -\mathbf{K}_\mathbf{x}^{-1}\mathbf{r}_\mathbf{x}. \tag{15}$$

This process is very efficient and fails only if the tangent stiffness matrix is singular. In a computational setting, this occurrence prevents the convergence of the iterative scheme based on the Newton–Raphson method. This situation can be get around by using the arc-length strategy suggested by Riks, see [23]. The key idea is the observation that the parameter used to describe the equilibrium curve, i.e. the load parameter λ, is unfit to describe the solution in a limit point, i.e. when the tangent stiffness matrix is singular. Riks' idea is to use as parameter to describe the equilibrium curve its arc-length.

[2] From Wikipedia [22]: "Raphson's most notable work is *Analysis Aequationum Universalis*, which was published in 1690. It contains a method, now known as the Newton–Raphson method, for approximating the roots of an equation. Isaac Newton had developed a very similar formula in his *Method of Fluxions*, written in 1671, but this work would not be published until 1736, nearly 50 years after Raphson's *Analysis*. However, Raphson's version of the method is simpler than Newton's, and is therefore generally considered superior. For this reason, it is Raphson's version of the method, rather than Newton's, that is to be found in textbooks today."

A simple derivation of one of the many variants of the Riks' strategy can be described assuming as starting point the expression of the residue in a first order Taylor expansion. We consider the pair $(\lambda, \mathbf{x})$ solution of the equilibrium problem, the pair $(\Delta\lambda, \Delta\mathbf{x})$ a suitable extrapolation of the solution starting from $(\lambda, \mathbf{x})$, and the pair $(\dot{\lambda}, \dot{\mathbf{x}})$ the correction capable of getting back the extrapolation on the equilibrium curve, in formula

$$\mathbf{r}(\mathbf{x} + \Delta\mathbf{x} + \dot{\mathbf{x}}, \lambda + \Delta\lambda + \dot{\lambda}) \approx \mathbf{r}_{\mathbf{x}+\Delta\mathbf{x}} + \mathbf{K}_{\mathbf{x}+\Delta\mathbf{x}}\dot{\mathbf{x}} - \dot{\lambda}\mathbf{p} = \mathbf{0}. \tag{16}$$

In order to balance the number of equations and the number of unknowns, we need to add one additional equation for computing $\dot{\lambda}$, i.e. a constraint equation. The most natural constraint is to search the solution on the circumference centred in $(\lambda, \mathbf{x})$ having as radius the fixed in advance arc-length. As often happens this choice is not so simple to code. From the computational point of view, a suitable general form of constraint is

$$\Delta\mathbf{x} \cdot \mathbf{C}\dot{\mathbf{x}} + \Delta\lambda\gamma\dot{\lambda} = 0, \tag{17}$$

where, besides the already defined quantities, we introduced the matrix $\mathbf{C}$ and the scalar γ. We remark that the condition (17) is a general orthogonality condition between extrapolation, i.e. the pair $(\Delta\lambda, \Delta\mathbf{x})$, and correction, i.e. the pair $(\dot{\lambda}, \dot{\mathbf{x}})$. By setting $\mathbf{C}$ and γ opportunely, we can improve the convergence or simplify the necessary calculations. Indeed, from Eq. (16) we can evaluate

$$\dot{\mathbf{x}} = \frac{\Delta\mathbf{x} \cdot \mathbf{C}\mathbf{K}^{-1}_{\mathbf{x}+\Delta\mathbf{x}}(\mathbf{r}_{\mathbf{x}+\Delta\mathbf{x}} - \dot{\lambda}\mathbf{p})}{\gamma\Delta\lambda + \Delta\mathbf{x} \cdot \mathbf{C}\mathbf{K}^{-1}_{\mathbf{x}+\Delta\mathbf{x}}\mathbf{p}}, \tag{18}$$

and, successively, by introducing Eq. (18) in Eq. (17), we can compute

$$\dot{\lambda} = \frac{\Delta\mathbf{x} \cdot \mathbf{C}\mathbf{K}^{-1}_{\mathbf{x}+\Delta\mathbf{x}}\mathbf{r}_{\mathbf{x}+\Delta\mathbf{x}}}{\gamma\Delta\lambda + \Delta\mathbf{x} \cdot \mathbf{C}\mathbf{K}^{-1}_{\mathbf{x}+\Delta\mathbf{x}}\mathbf{p}}. \tag{19}$$

At this point, we can make as choice for $(\gamma, \mathbf{C})$ the pair $(0, \mathbf{K}_{\mathbf{x}+\Delta\mathbf{x}})$ in order to obtain a very simple formula for the correction $(\dot{\lambda}, \dot{\mathbf{x}})$. By introducing this choice in Eq. (19), we have

$$\dot{\lambda} = \frac{\Delta\mathbf{x} \cdot \mathbf{r}_{\mathbf{x}+\Delta\mathbf{x}}}{\Delta\mathbf{x} \cdot \mathbf{p}}, \tag{20}$$

and successively compute $\dot{\mathbf{x}}$ by means Eq. (18). We remark that the *a priori* choice $\dot{\lambda} = 0$ furnishes exactly the Newton–Raphson algorithm.

The algorithm sketched in the foregoing requires a first extrapolation in each step. The simplest way is to extrapolate a solution guess on the basis of the previous step $(\Delta\lambda_p, \Delta\mathbf{u}_p)$, in formulae:

$$\begin{aligned} \Delta\lambda &= m\Delta\lambda_p, \\ \Delta\mathbf{u} &= m\Delta\mathbf{u}_p, \end{aligned} \tag{21}$$

where we introduced an adaptive coefficient m capable of modifying, increasing or decreasing, the arc-length during the step-by-step procedure on the basis of the convergence velocity in the previous step. As proposed in [24], the adaptive coefficient m can be written as

$$m = 1 - \frac{r - n}{r + n}, \tag{22}$$

r and n being the numbers of required and needed loops, respectively. At the beginning, the first step, we set $m = 1$. The choice of the initial value of $\Delta\lambda$ automatically fixes the initial arc-length value and can be used to evaluate the initial $\Delta\mathbf{x}$.

4. Some numerical simulations

We describe a group of numerical simulations concerning curved pantographs based on Piñero and Hoberman unit cells. By using the digital twin built with the model sketched in Section 2 and the solution strategy defined in Section 3, we perform some numerical simulations aiming to prove: (i) the deployability of some curved pantographs and (ii) the mechanical response under relevant load conditions.

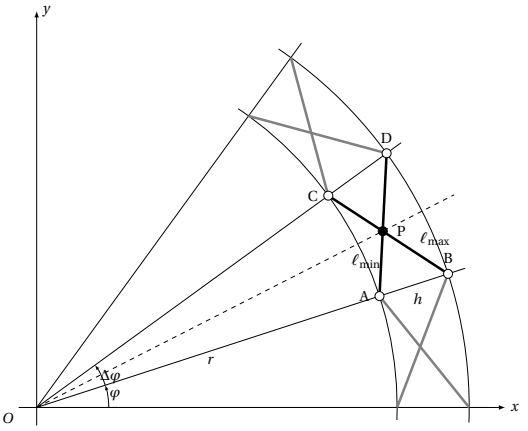

Figure 5. Pantographic circular arc made by Piñero unit cells: geometrical parameters.

Firstly, we consider a piece of annulus delimited by two concentric circles of radii r and $r+h$ and by the angles φ and $\varphi+\Delta\varphi$, see Figure 5. The points A, B, C and D are perfectly determined, for instance from their polar coordinates, therefore the pivot P for the Piñero unit cell can be computed by the intersection of the segments AD and BC both of length $\ell = \|D-A\| = \|C-B\|$. The pivot P splits the segments AD and BC in two pairs of segments of lengths $\ell_{\min}$ and $\ell_{\max}$ which can be determined by the relations

$$\begin{aligned} \ell_{\min} &= \frac{r\ell}{h+2r}, \\ \ell_{\max} &= \ell - \ell_{\min}. \end{aligned} \tag{23}$$

For the unit cell proposed by Hoberman, see Figure 6, it is simple to prove, see [8] for a complete proof, that the polar coordinate of the pivot P are

$$\left(\frac{2r+h}{2\cos\left(\varphi - \frac{\Delta\varphi}{2}\right)}, \varphi + \frac{\Delta\varphi}{2} \right). \tag{24}$$

Geometrical relations (23) and (24) are used to build the mechanical digital twin of some simple curved pantographs for analysing some case studies reported hereafter, see also [25].

4.1. *Semicircular pantographic arcs following Piñero and Hoberman unit cells: from unfold to fold positions*

Using the geometrical and mechanical data reported in Table 1, we built the data for two semicircular pantographic arcs following Piñero and Hoberman unit cells. For both semicircular arcs, we performed a numerical simulation locking the node with polar coordinates $(r,0)$ and imposing a horizontal displacement ruled by the multiplier λ on the node with polar coordinates $(r+h,0)$, see Figures 5 and 6.

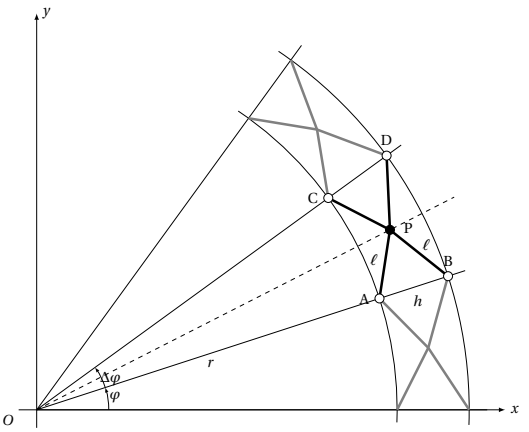

Figure 6. Pantographic circular arc made by Hoberman unit cells: geometrical parameters.

Table 1. Geometrical and mechanical data used for the pantographic semicircular arc numerical simulations in the MKS system of units.

inner radius r	**thickness h**	**spring stiffness a**	**angle spring stiffness b**
10	1	10^3	10^3

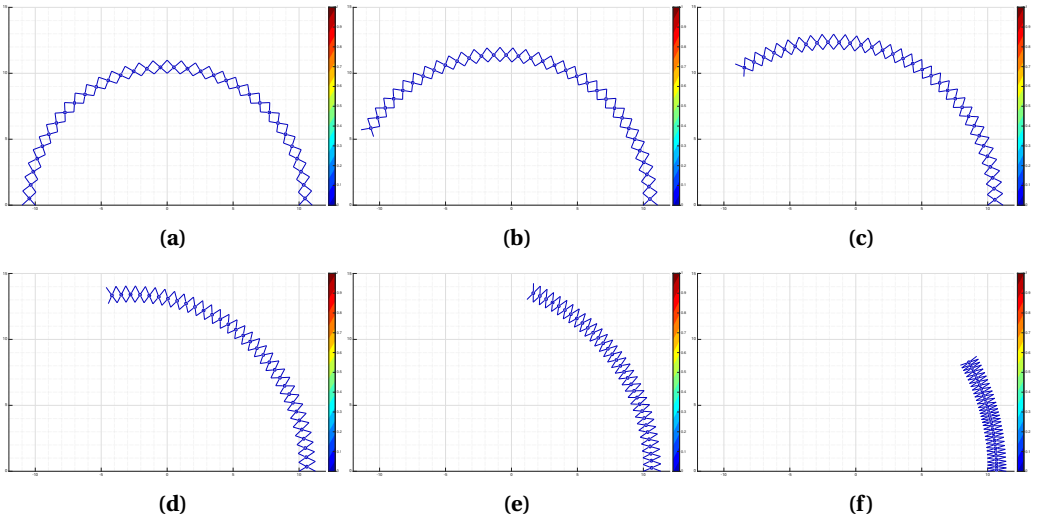

Figure 7. Stroboscopic shoots, (a)–(f), showing the absence of strains on springs and angle springs of the pantographic arc based on Piñero unit cell.

As is clearly visible from Figures 7 and 8, the stroboscopic shoots from the unfold to the fold configurations for the Piñero and Hoberman unit cells, respectively, show that all the springs used to model the pantographic arcs are not interested from strain as is proved by the colour blue corresponding, see also the colour bar, to zero strain in all the considered configurations.[3]

[3]In the supplementary materials of this work there are two brief videoclips, `Pinero32deployability.mp4` and `Hoberman32deployability.mp4`, for the Piñero and Hoberman unit cells, respectively, which show the complete

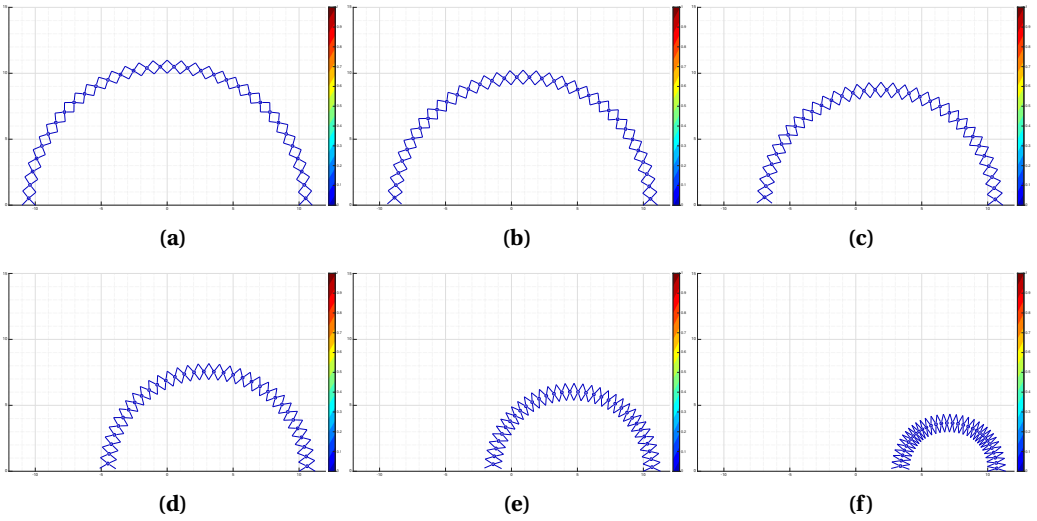

Figure 8. Stroboscopic shoots showing the absence of strains on springs and angle springs of the pantographic arc based on Hoberman unit cell.

We remark that in the whole unfold to fold process the two considered unit cells behave in different manner: the semicircular Piñero pantographic arc becomes an arc of circumference with a smaller angle at the centre whereas that based on the Hoberman unit cell preserves the shape, semicircular, but reduces the radius.

4.2. *Clamped-clamped semicircular pantographic arcs*

After the test on the deployability, we consider some numerical simulations aiming to discover the mechanical behaviour under standard constraints and loads. In this perspective, we consider again the semicircular pantographic arcs following Piñero and Hoberman unit cells using the geometrical and mechanical data reported in Table 1. Further, we assume that the displacements on the left and on the right end nodes are prevented by constraints, i.e. four external hinges.[4] As load conditions we consider:

Case study 1: a uniform vertical load, from top to bottom, on each one unit cell pivot;
Case study 2: a uniform horizontal load, from right to left, on each one unit cell pivot of the half right side;
Case study 3: a uniform vertical load, from top to bottom, on each one unit cell pivot of the half right side.

Case study 1. Figure 9 reports the λ-evolution of the midpoint displacement of the inner circle, the reactions on each one of the two right end constrained nodes and the strain energy, split in that of springs and of angle springs, for the semicircular arcs based on Piñero and Hoberman unit cells. Figure 10 reports six stroboscopic shoots reporting the deformation and the strain energy level on each spring and angle spring of the considered pantographic arcs. For both analysed

evolution from the unfold to the fold configurations.

[4] Although below it is not discussed the sensitivity of the response to the kind and number of constraints, this is a relevant task for multifunctional pantographic metamaterials, see [26], where boundary conditions and coupling mechanisms are shown to play a crucial role in determining the global response.

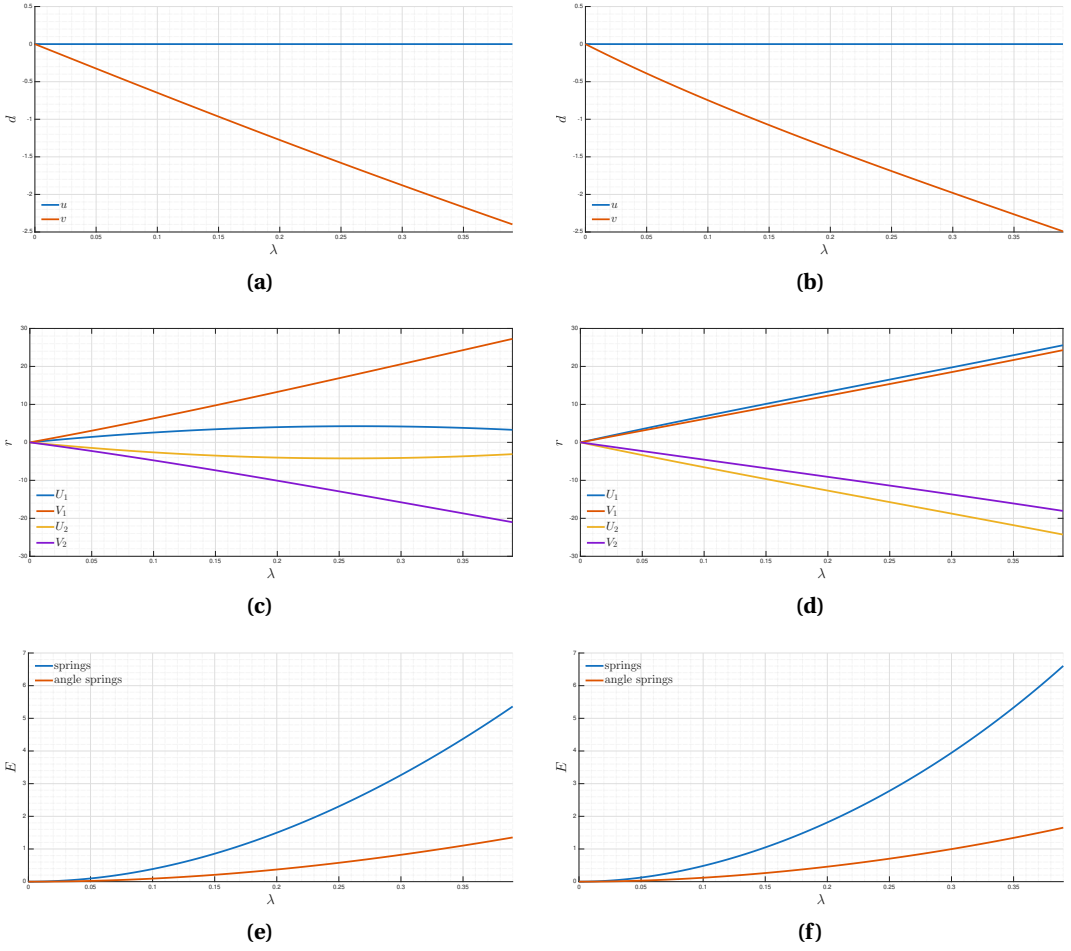

Figure 9. Case study 1: displacements of the midpoint inner node, reaction on the right end nodes and strain energy evolution, split in that of springs and angle springs, for Piñero, on the left side, and Hoberman, on the right side.

kinds of pantographic arcs, the complete load evolution processes are reported in the videoclips `Pinero32v.mp4` and `Hoberman32v.mp4` available in the supplementary materials of this work.

We remark that in this comparison:

(1) there is a slight difference on the vertical displacement of the arc mid node, more precisely this displacement is bigger in the Hoberman pantographic arc;
(2) the horizontal reactions of the two considered nodes are very different both in their magnitude and in the λ-evolution; less pronounced is the difference on the vertical reactions;
(3) the strain energy, both the part associated with the springs and the part associated with the angle springs, is higher for the Hoberman scheme.

Case study 2. As second numerical simulation, we consider the same geometry, constraints and mechanical parameters used for the previous case study. As load case, we consider a uniform horizontal force $-\lambda$, i.e. from right to left, on the pivots of the right side of the arcs. Figure 11 reports the λ-evolution of the midpoint displacement of the inner circle, the reactions on each

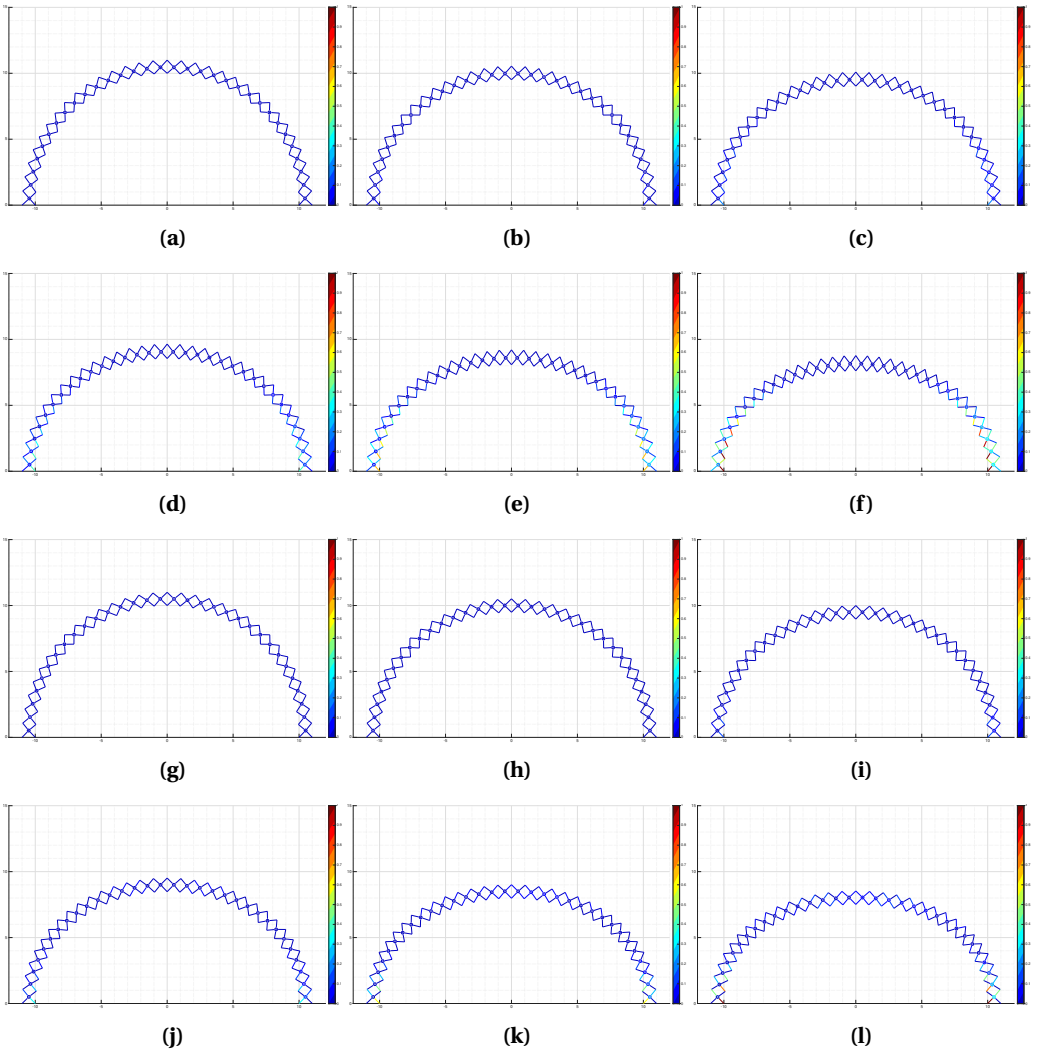

Figure 10. Case study 1: stroboscopic shoots showing the strain energy level on springs and angle springs for Piñero (a)–(f) and Hoberman (g)–(l) unit cells.

one of the two right end constrained nodes and the strain energy, split in that of springs and angle springs, for the semicircular arcs based on Piñero and Hoberman unit cells. Figure 12 reports six stroboscopic shoots showing the deformation of the pantographic arc and the strain level on each spring and angle spring. Also in this case study, for both analysed kinds of pantographic arcs, the complete load evolution processes are reported in the videoclips `Pinero32hh.mp4` and `Hoberman32hh.mp4` available in the supplementary materials of this work.

From the analysis of this case study, we remark that:

(1) the Hoberman scheme has displacements notably higher than the Piñero scheme;
(2) there are no significant differences for the reactions;
(3) the strain energy of the springs is remarkably higher for the Hoberman scheme whereas the angle strain energy is comparable.

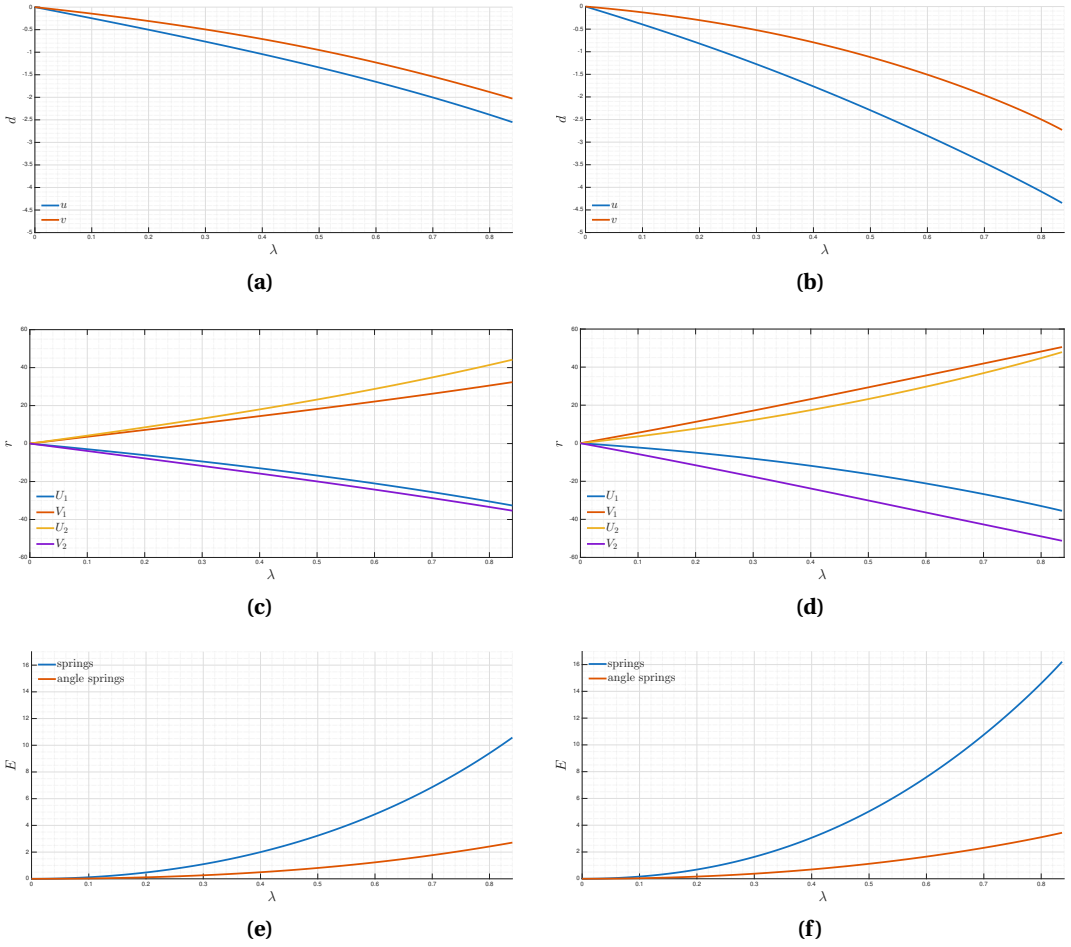

Figure 11. Case study 2: displacements of the midpoint inner node, reaction on the right end nodes and strain energy evolution, split in that of springs and angle springs, for Piñero, on the left side, and Hoberman, on the right side.

Case study 3. As third numerical simulation we consider the same geometry, constraints and mechanical parameters used for the previous two case studies but consider as load case a uniform vertical force $-\lambda$, i.e. from top to bottom, on the pivots of right side of the arcs. Figure 13 reports the λ-evolution of midpoint node displacements, that of the reactions on each one of the two right end constrained nodes and that of the strain energy, split in that of springs and that of angle springs, for the semicircular arcs based on Piñero and Hoberman unit cells.

Figure 14 reports six stroboscopic shoots showing the deformation of the pantographic arc and the strain energy level on each spring and angle spring. Also for this case study, for both analysed kinds of pantographic arcs, the complete load evolution processes are reported in the videoclips `Pinero32hv.mp4` and `Hoberman32hv.mp4` available in the supplementary materials of this work.

For this case study we observe:

(1) higher displacements for the Hoberman scheme which also reveal a remarkably nonlinear behaviour;
(2) qualitative and quantitative, remarkably, differences in the reactions;

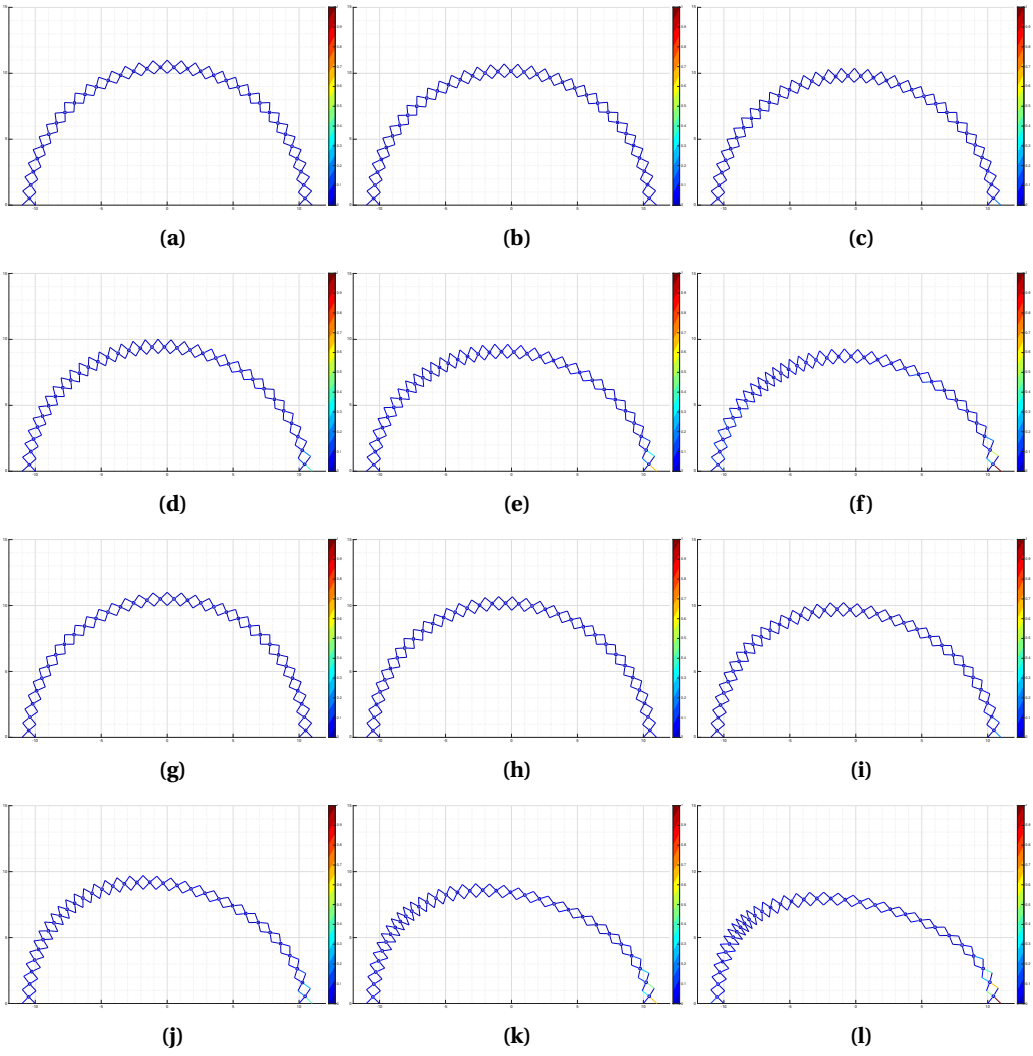

Figure 12. Case study 2: stroboscopic shoots showing the strain energy levels on springs and angle springs for Piñero (a)–(f) and Hoberman (g)–(l) unit cells.

(3) remarkable quantitative differences for the strain energy of springs, higher in the Hoberman scheme, and comparable for the angle springs.

5. Concluding remarks and future challenges

Freely inspired by some deployable structures based on an enlarged vision of the pantographic unit cell, in particular those proposed by Piñero and Hoberman, and by the reading of the seminal paper of You and Pellegrino, we started the study of curved pantographic structures being sure that the same ideas at the basis of deployable structures can be fruitfully used for the design of metamaterials.

In order to have a tool for performing mechanical experiments, we first built a digital twin capable of describing the essential characteristic of the mechanical response. The main peculiarities of the digital twin are: (i) the simplicity; (ii) the use of few elementary *bricks*; (iii) the capabil-

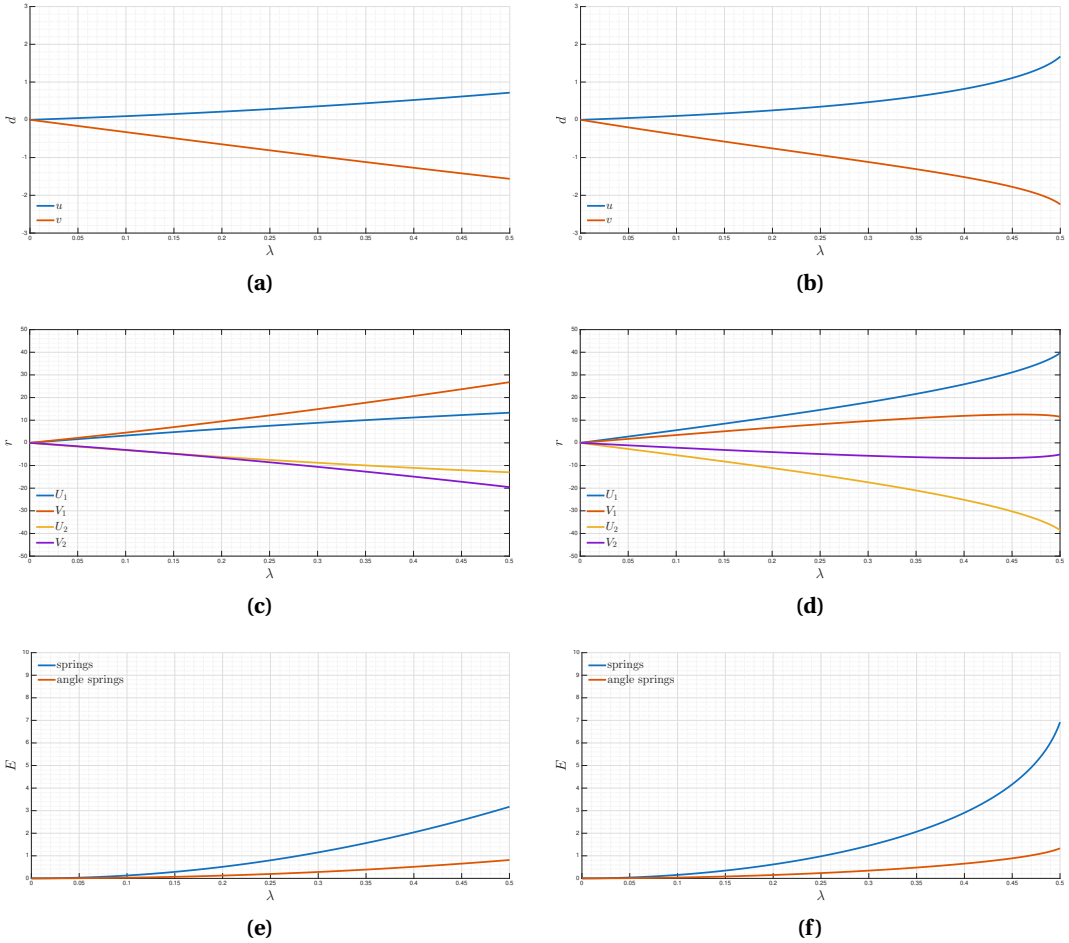

Figure 13. Case study 3: displacements of the midpoint inner node, reaction on the right end, node 1 and 2, and strain energy evolution, split in that of springs and angle springs, for Piñero, on the left side, and Hoberman, on the right side.

ity to explore the mechanical behaviour for large displacements. All these requests are satisfied by a discrete element model based on springs and angle springs to model the nonlinear interactions in-between pairs and triplets of points.[5]

We remark that the model presented in the foregoing is also capable of analysing spring network very different from those of pantographic structures, see, e.g., [14,15], where the same model is used to perform numerical experiments useful for building continuum model, see, e.g., [28–31], of beams with exotic mechanical behaviour.

The mechanical digital twin was successively used to begin some experiences on semicircular pantographic arcs built on the basis of Piñero and Hoberman unit cells. In particular, we tested the deployability, i.e. the existence of a zero energy mode, and the mechanical behaviour under some common loading conditions when the zero energy mode is prevented by a large enough number of well-posed constraints.

[5] An alternative approach which surely deserves to be exploited is that proposed in [27] which uses the swarm dynamics to describe pantographic structures by, using the authors' words, "a discrete two-dimensional *kinematic* model".

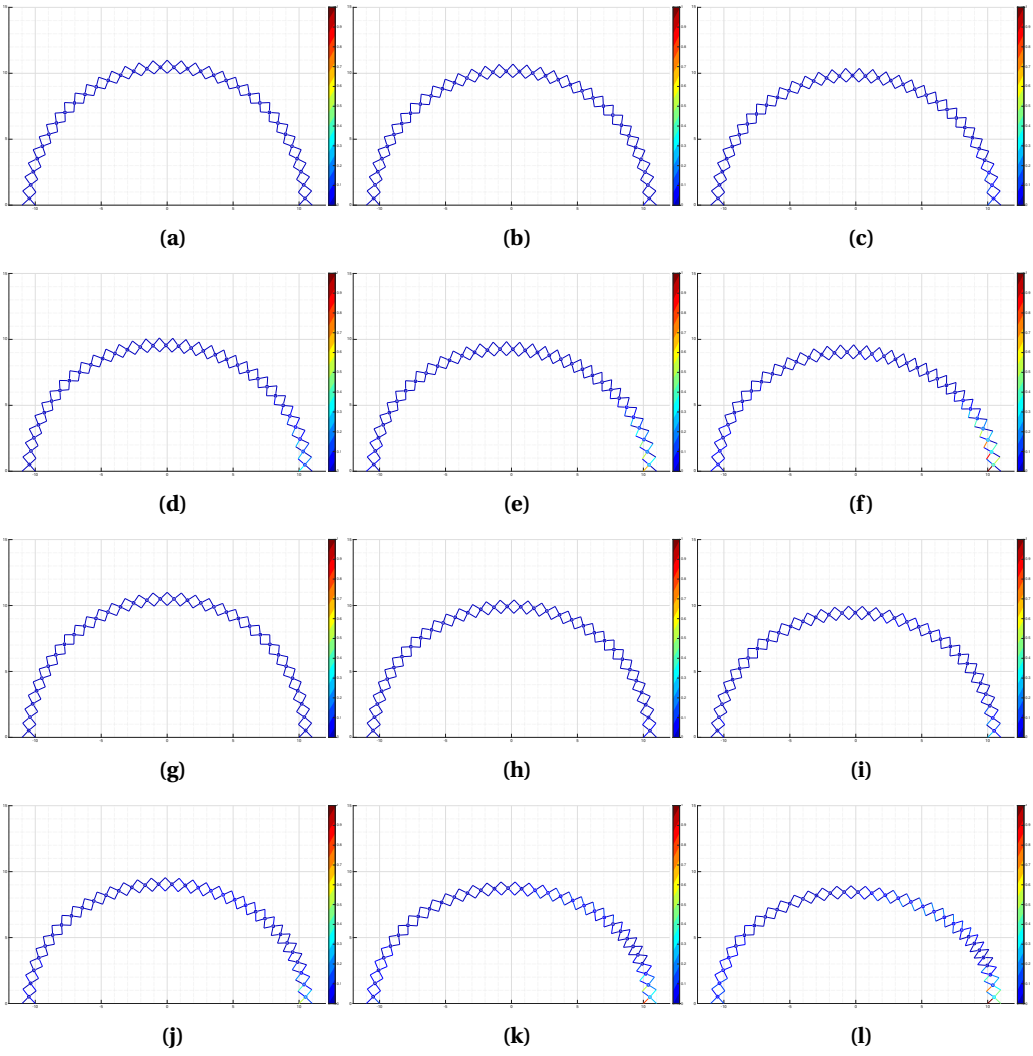

Figure 14. Case study 3: stroboscopic shoots showing the strain energy levels on springs and angle springs for Piñero (a)–(f) and Hoberman (g)–(l) unit cells.

The pantographic curves presented above have several interesting applications. As examples, we suggest two possible fields, one concerning the development of new metamaterials with enhanced mechanical properties and one useful in the conception of robotic arms. In the former case, pantographic curves can be thought of as fibres inserted in a composite metamaterials or as elements of a hierarchical organisation. In the latter case, pantographic curves have a natural application in the field of robotic arms since their beams, pivots and hinges can be controlled by means of actuators capable, e.g., of varying the angle in-between beams, therefore the whole configuration of the robotic arm.

Future challenges concern the following issues:

(1) the performing of physical experiments using the potentiality of the 3D print technology and of the digital image correlation, see [32];
(2) the extension of the presented model for including damaging analyses, see [33–35];

(3) the extension to full three-dimensional model; the Piñero pantographic unit cell used for the deployable theatre roof is very challenging and might give surprising results in the design of metamaterials as well as the Hoberman unit cell which has a mechanical behaviour somewhat different from that of Piñero;
(4) the optimisation of the mechanical behaviour, see, e.g., [36];
(5) the extension to cases where the inertial forces are not negligible [37];
(6) the generalisation of the present approach to problems characterised by nonlocal effects, see [38–41];
(7) the identification and validation of the constitutive parameters of the model, see [42];
(8) the exploration of deployable structures such as that sketched by Tůma, see [43], which is also the link in-between pantographic and tensegrity structures, see [44];
(9) the application to the modern orthodontic techniques, see, e.g., [45];
(10) the study of complex pantographic curves, see [46,47] for a modern representation of curves, such as presented in Figure 15, see also [48], in order to use them in the spirit presented in [49].

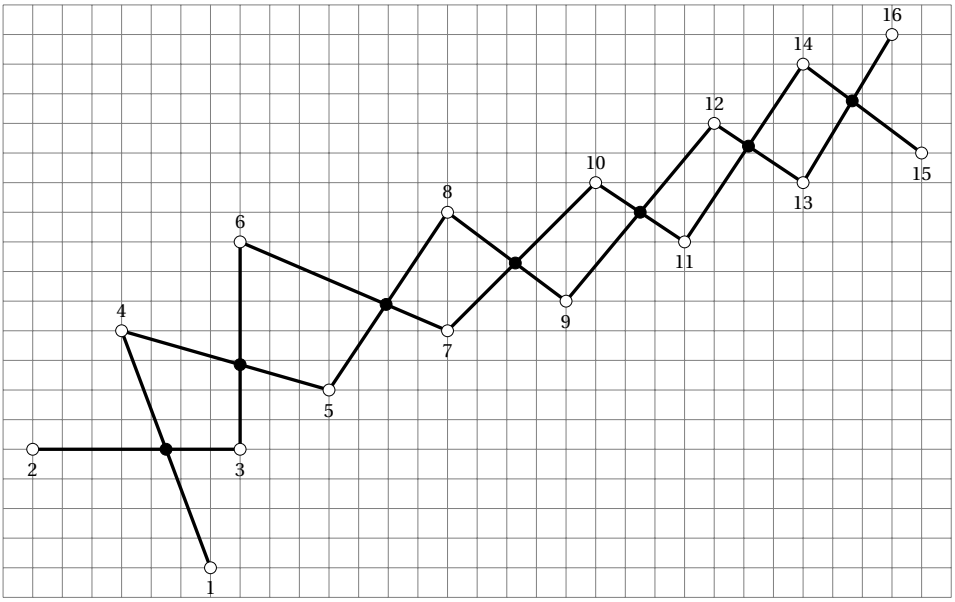

Figure 15. Curved pantograph following generalised Piñero unit cell.

Declaration of interests

The author does not work for, advise, own shares in, or receive funds from any organization that could benefit from this article, and has declared no affiliations other than their research organizations.

Supplementary material

Supporting information for this article is available on the journal's website under https://doi.org/10.5802/crmeca.352 or from the author.

References

[1] F. dell'Isola, P. Seppecher, M. Spagnuolo, et al., "Advances in pantographic structures: design, manufacturing, models, experiments and image analyses", *Contin. Mech. Thermodyn.* **31** (2019), no. 4, pp. 1231–1282.

[2] F. dell'Isola, P. Seppecher, J.-J. Alibert, et al., "Pantographic metamaterials: an example of mathematically driven design and of its technological challenges", *Contin. Mech. Thermodyn.* **31** (2019), no. 4, pp. 851–884.

[3] J.-J. Alibert, P. Seppecher and F. dell'Isola, "Truss modular beams with deformation energy depending on higher displacement gradients", *Math. Mech. Solids* **8** (2003), no. 1, pp. 51–73.

[4] A.-n. Abd-alla, I. Giorgio, L. Galantucci, A. M. Hamdan and D. Del Vescovo, "Wave reflection at a free interface in an anisotropic pyroelectric medium with nonclassical thermoelasticity", *Contin. Mech. Thermodyn.* **28** (2016), no. 1, pp. 67–84.

[5] M. Spagnuolo, K. Barcz, A. Pfaff, F. dell'Isola and P. Franciosi, "Qualitative pivot damage analysis in aluminum printed pantographic sheets: Numerics and experiments", *Mech. Res. Commun.* **83** (2017), pp. 47–52.

[6] A. Ciallella, G. La Valle, A. Vintache, B. Smaniotto and F. Hild, "Deformation mode in 3-point flexure on pantographic block", *Int. J. Solids Struct.* **265–266** (2023), article no. 112129 (14 pages).

[7] S. Moschini, L. Murcia Terranova and F. D'Annibale, "Kinematics of zigzagged articulated parallelograms with articulated braces (ZAPAB) mechanisms", *Math. Mech. Complex Syst.* **13** (2025), no. 4, pp. 471–500.

[8] Z. You and S. Pellegrino, "Foldable bar structures", *Int. J. Solids Struct.* **34** (1997), no. 15, pp. 1825–1847.

[9] E. P. Piñero, Estructura reticular estérea plegable, Spain patent, no. ES266801A1, 1961.

[10] C. Hoberman, Reversibly expandable doubly-curved truss structure, US patent, no. US4942700A, 1990.

[11] C. Hoberman, Radial expansion/retraction truss structures, US patent, no. US5024031A, 1991.

[12] L. Murcia Terranova, "Planar one-dimensional continua whose energy depends on the gradient of curvature: an overview of their applications in metamaterials design", *Math. Mech. Complex Syst.* **13** (2025), no. 2, pp. 127–166.

[13] L. Placidi, U. Andreaus, A. Della Corte and T. Lekszycki, "Gedanken experiments for the determination of two-dimensional linear second gradient elasticity coefficients", *Z. Angew. Math. Phys.* **66** (2015), no. 6, pp. 3699–3725.

[14] F. dell'Isola, S. Moschini and E. Turco, "Towards the synthesis of planar beams whose deformation energy depends on the third gradient of displacement", *Math. Mech. Complex Syst.* **12** (2024), no. 4, pp. 573–597.

[15] L. Murcia Terranova, E. Turco, A. Misra and F. dell'Isola, "Computational identification of double-bending stiffness: from Zigzagged Articulated Parallelograms with Articulated Braces (ZAPAB) structures to pure-curvature gradient planar inextensible 1D continua", *Comptes Rendus. Mécanique* **353** (2025), pp. 647–672.

[16] I. Berinskii and V. A. Eremeyev, "On the continuum modeling of the foldable rod with rigid links", *Mech. Res. Commun.* **150** (2025), article no. 104574 (8 pages).

[17] F. dell'Isola, D. Steigmann, A. Della Corte, et al., *Discrete and continuum models for complex metamaterials*, Cambridge University Press, 2020.

[18] B. E. Abali, "Energy based methods applied in mechanics by using the extended Noether's formalism", *Z. Angew. Math. Mech.* **103** (2023), no. 12, article no. e202300020 (23 pages).

[19] K. Liu and G. H. Paulino, "Nonlinear mechanics of non-rigid origami: an efficient computational approach!", *Proc. R. Soc. Lond., A, Math. Phys. Eng. Sci.* **473** (2017), no. 2206, article no. 20170348 (28 pages).

[20] E. Turco, E. Barchiesi and F. dell'Isola, "Nonlinear dynamics of origami metamaterials: energetic discrete approach accounting for bending and in-plane deformation of facets", *Z. Angew. Math. Phys.* **74** (2023), no. 1, article no. 26 (29 pages).

[21] E. Turco, F. dell'Isola, A. Cazzani and N. Rizzi, "Hencky-type discrete model for pantographic structures: numerical comparison with second gradient continuum models", *Z. Angew. Math. Phys.* **67** (2016), no. 4, article no. 85 (28 pages).

[22] "Joseph Raphson", in *Wikipedia*, 2026. Online at https://en.wikipedia.org/wiki/Joseph_Raphson (accessed on March 17, 2026).

[23] E. Riks, "The Application of Newton's Method to the Problem of Elastic Stability", *J. Appl. Mech.* **39** (1972), no. 4, pp. 1060–1065.

[24] M. J. Clarke and G. J. Hancock, "A study of incremental-iterative strategies for non-linear analyses", *Int. J. Numer. Methods Eng.* **29** (1990), no. 7, pp. 1365–1391.

[25] J. Chróścielewski and V. A. Eremeyev, "Can we really solve an arch stability problem?", *Int. J. Eng. Sci.* **194** (2024), article no. 103968 (13 pages).

[26] M. Spagnuolo, "Coupled Mechanical–Electrical modeling of pantographic metamaterials with simplified flexoelectric bending", *Continuum Mechanics and Thermodynamics* **37** (2025), no. 6, article no. 96.

[27] P. D'Avanzo, A. C. Rapisarda and R. Dell'Erba, "An approach to the mechanics of pantographic structures through swarm dynamics", *Mathematics and Mechanics of Solids* **30** (2025), no. 7, pp. 1471–1495.

[28] N. M. Cordero, S. Forest and E. P. Busso, "Second strain gradient elasticity of nano-objects", *J. Mech. Phys. Solids* **97** (2016), pp. 92–124.

[29] F. Fabbrocino, H. Darban and R. Luciano, "Nonlocal layerwise formulation for interfacial tractions in layered nanobeams", *Mech. Res. Commun.* **109** (2020), article no. 103595.
[30] F. dell'Isola, S. R. Eugster, R. Fedele and P. Seppecher, "Second-gradient continua: from Lagrangian to Eulerian and back", *Math. Mech. Solids* **27** (2022), no. 12, pp. 2715–2750.
[31] R. Alicandro, A. Braides, M. Cicalese and M. Solci, *Discrete variational problems with interfaces*, Cambridge Monographs on Applied and Computational Mathematics, vol. 40, Cambridge University Press, 2024.
[32] R. Fedele, "Simultaneous Assessment of Mechanical Properties and Boundary Conditions Based on Digital Image Correlation", *Exp. Mech.* **55** (2015), no. 1, pp. 139–153.
[33] L. Placidi, E. Barchiesi and A. Misra, "A strain gradient variational approach to damage: a comparison with damage gradient models and numerical results", *Math. Mech. Complex Syst.* **6** (2018), no. 2, pp. 77–100.
[34] M. Spagnuolo, M. E. Yildizdag, X. Pinelli, A. Cazzani and F. Hild, "Out-of-plane deformation reduction via inelastic hinges in fibrous metamaterials and simplified damage approach", *Math. Mech. Solids* **27** (2022), no. 6, pp. 1011–1031.
[35] M. E. Yildizdag, L. Placidi and E. Turco, "Modeling and numerical investigation of damage behavior in pantographic layers using a hemivariational formulation adapted for a Hencky-type discrete model", *Contin. Mech. Thermodyn.* **35** (2022), no. 4, pp. 1481–1494.
[36] B. Desmorat, M. Spagnuolo and E. Turco, "Stiffness optimization in nonlinear pantographic structures", *Math. Mech. Solids* **25** (2020), no. 12, pp. 2252–2262.
[37] V. A. Eremeyev and I. Elishakoff, "On rotary inertia of microstuctured beams and variations thereof", *Mech. Res. Commun.* **135** (2024), article no. 104239 (7 pages).
[38] A. Braides and M. Solci, "Compactness by Coarse-Graining in Long-Range Lattice Systems", *Adv. Nonlinear Stud.* **20** (2020), no. 4, pp. 783–794.
[39] A. Braides, A. Causin and M. Solci, "Discrete approximation of nonlocal-gradient energies", *Adv. Calc. Var.* **17** (2024), no. 4, pp. 1507–1518.
[40] C. Boutin, "Microstructural effects in elastic composites", *Int. J. Solids Struct.* **33** (1996), no. 7, pp. 1023–1051.
[41] F. dell'Isola, U. Andreaus and L. Placidi, "At the origins and in the vanguard of peridynamics, non-local and higher-gradient continuum mechanics: an underestimated and still topical contribution of Gabrio Piola", *Math. Mech. Solids* **20** (2015), no. 8, pp. 887–928.
[42] M. De Angelo, N. Yilmaz, M. E. Yildizdag, A. Misra, F. Hild and F. dell'Isola, "Identification and validation of constitutive parameters of a Hencky-type discrete model via experiments on millimetric pantographic unit cells", *Int. J. Non-Linear Mech.* **153** (2023), article no. 104419.
[43] J. Tůma, "Pantograph concept", in *FLOW*, Studio Florián, 2011. Online at https://www.studioflorian.com/projekty/145-jan-tuma-pantograph-concept.
[44] F. Fraternali, L. Senatore and C. Daraio, "Solitary waves on tensegrity lattices", *J. Mech. Phys. Solids* **60** (2012), no. 6, pp. 1137–1144.
[45] P. Kurzeja, I. Giorgio and M. Tepedino, "Mechanical in-silico modeling of orthodontic tooth movement: A review of the boundary value problem", *Math Mech Solids* (2025), article no. 10812865251369422 (37 pages). Online first.
[46] L. Greco, M. Cuomo, L. Contrafatto and S. Gazzo, "An efficient blended mixed B-spline formulation for removing membrane locking in plane curved Kirchhoff rods", *Comput. Methods Appl. Mech. Eng.* **324** (2017), pp. 476–511.
[47] L. Greco, M. Cuomo and L. Contrafatto, "A reconstructed local $\overline{B}$ formulation for isogeometric Kirchhoff–Love shells", *Comput. Methods Appl. Mech. Eng.* **332** (2018), pp. 462–487.
[48] D. Rosenberg, "Indeterminate architecture: Scissor-pair transformable structures", *Footprint* **4** (2010), no. 6, pp. 19–39.
[49] A. Ciallella, F. D'Annibale, D. Del Vescovo and I. Giorgio, "Deformation patterns in a second-gradient lattice annular plate composed of "Spira mirabilis" fibers", *Contin. Mech. Thermodyn.* **35** (2023), no. 4, pp. 1561–1580.